A Finite Element Approach to Evaluate and Predict the Shear Capacity of Steel Fiber-Reinforced Concrete Beams

Laith N. Hussain
Civil Engineering Department, University of Technology, Iraq
bce.20.74@grad.uotechnology.edu.iq

Mohammed J. Hamood
Civil Engineering Department, University of Technology, Iraq
40040@uotechnology.edu.iq

Ehsan A. Al-Shaarbaf
Civil Engineering Department, Al-Esraa University College, Iraq
ishaarbaf@esraa.edu.iq

Received: 19 May 2023 | Revised: 13 June 2023 | Accepted: 26 June 2023

 DOI: https://doi.org/10.48084/etasr.6054

ABSTRACT

Adding steel fibers to a concrete matrix enhances the shear capacity of reinforced concrete beams. A comprehensive understanding of this phenomenon is essential to evaluate engineering designs accurately. The shear capacity of Steel Fiber Reinforced Concrete (SFRC) beams is affected by many parameters, such as the ratio of the shear span to the effective depth of the SFRC beam, the compressive strength of concrete, the longitudinal reinforcement ratio, volume fraction, aspect ratio, and the type of fibers. Therefore, to cover the influence of these parameters on the shear capacity of SFRC beams, 91 beams from previous studies, divided into 10 groups, were considered in the current study. Two approaches have been used to predict the shear capacity of SFRC beams. The first approach used 7 predicting equations derived from previous studies and the second one used finite element analysis (ANSYS software) to simulate the 91 beams. Despite the many approaches to simulate the structure elements, there is no reliable approach able to simulate satisfactorily 91 SFRC beams as this study does. The log file of ANSYS software was used to simulate and calculate the shear strength capacity of the beams. The results show a reasonable agreement with the experimental tests. The extracted results were much closer and more realistic than those obtained by the predicting equations. Also, the χ factor (squared value of experimental shear capacity to the predicted shear capacity) of the ANSYS software results is 97%, while the closest proposed equation gives 91%.

Keywords-fibers; experimental shear capacity; ANSYS; predicting shear equation

I. INTRODUCTION

Poor toughness of high-strength concrete can be overcome with the addition of short discontinuous fibers. Fibers control the propagation of cracks and limit the crack width. The high elastic modulus of steel fibers also enhances concrete's flexural toughness and ductility. The participation of steel fibers can be seen mainly after matrix cracking in concrete. However, adding steel fibers at high dosages has a prospective impediment in terms of poor workability and growth cost. In addition, the increased stiffness of steel fibers and micro-defects such as voids and honeycombs may form during placing due to inadequate consolidation at the low workability stage [1, 2]. A compromise of the concrete mixture properties to gain good fresh concrete properties (in reduced early-age cracking and workability) and the toughness of hardened concrete can be reached by adding two different fiber types, which can function individually at different volume fractions to yield optimum performance. The addition of steel fibers to the concrete matrix results in excellent fresh concrete properties and deducts micro cracks [3]. The hybrid combination of metallic and non-metallic fibers can offer potential advantages in improving concrete properties and reducing the cost of concrete production. When the volume fraction of the fibers is increased, it results in denser and more uniform distribution of the fibers throughout the concrete, reducing shrinkage cracks and improving concrete post-crack strength. In addition, it is essential to have a combination of low and high-modulus fibers to arrest the micro and macro cracks, respectively. Another

beneficial variety of threads is that of long and short fibers. Using different lengths of fibers would control different scales of cracking [4-7].

There are many challenges when conducting finite element analysis for many beams or for beams of complicated geometry [8-10]. The nonlinear finite element technique was utilized in this work to predict the shear capacity of 91 SFRC beams and evaluate the accuracy of the proposed equations by previous studies to calculate the shear capacity SFRC beams [11-13]. A new nonlinear finite element approach was built in ANSYS software to model the selected data involving SFRC beams with different parameters such as the ratio of shear span to the effective depth of the SFRC beam, compressive strength of concrete, longitudinal reinforcement ratio, volume fraction, aspect ratio, and type of used fibers [14-16]. According to the experimental work, concentrated load was applied in different shear spans. One support prevents the movement in the X and Z directions and the translation in the Y direction acted as a pin support. The second support prevents the movement in the X direction and prevents the translation in the Y direction to act as roller support.

TABLE I. THE CONSIDERED SHEAR STRENGTH EQUATIONS FOR SFRC BEAMS

Ref.	Shear strength expression
[17]	$Vn = kf\ ct(d/a)^{1/4}\ bd$, where k = 2/3, f_{ct} is the FRC split cylinder strength,and a is the shear span. If f_{ct} is unknown, it can be taken as $f_{ct} = 0.79\sqrt{f'c}\ (MPa)$.
[18]	$Vn = \{[0.16\sqrt{f'c} + 17.2_{\rho}(Vd/M)] + \sigma_{tu}\}bd$, where V and M are the shear and moment capacity at critical section, and σ_{tu} is the FRC post crack tensile stress. For beams with $a/d \geq 2$ subjected to a concentrated load placed at a distance a from support, $M/V = (Mmax/V) — d = a - d$ where M_{max} is the moment at the section the concentrated load is applied. For specimen tested in [17] the σ_{tu} values used for all specimens was calculated as, $\sigma_{tu} = 0.41\tau F$, where fibre-matrix bond τ was taken as $0.68\sqrt{f'c}$, as recommended in [20] and $F = (Lf/Df)/Vf\ df$, where $Lf, Df,$ and Vf are the length, the diameter, and the volume fraction the used fiber, respectively, and df = 1 for the hooked steel fibers.
[19]	$Vn = \{e[A'f\ spf\ c + B'\rho(d/a)] + vb\}bd$, where e = 1.0 for a/d > 2.8 and e = 2.8 d/a when $a/d \leq 2.8$, ρ is the ratio of longtudinal reinforcement, A' = 0.24, B' = 80 MPa, $f_{spf\ c} = [f_{cuf}/(20 —\sqrt{F})] + B + C\sqrt{F}$,where f_{cuf} is the FRC cube strength, B = 0.7 MPa, C = 1 MPa, and $v_b = 0.41\tau F$, where τ is the fiber interficil bond assumed as 4.15 MPa.
[20]	$V_n = (2.11p3\sqrt{f'c}+7F)[\rho(d/a)^{1/3}]bd$, where $a/d \geq 2.5$.
[21]	$V_n = [0.167e + 0.25F]\sqrt{f'c}bd$, where e = 1.0 for a/d > 2.5 and e = $2.5d/a$ when $a/d \leq 2.5$.
[22]	$V_n = \{3.7ef_{spfc}^{2/3}\ [\rho(d/a)^{1/3}] + 0.8v_b\}bd$, where e = 1.0 for a/d > 3.4 and e = $3.4d/a$ when $a/d \leq 3.4$. $f_{spf\ c} = [f_{cuf}/(20 — \sqrt{F})] + B + C\ F$, where f_{cuf} is the FRC cube strength, B = 0.7 MPa, and C = 1 MPa/ $V_b = 0.41\tau F$, where τ = fibre-matrix interfacial bond,assumed equal to 4.15 MPa.
[23]	$V_n = (0.11f'c\ \beta_1\ cb + (\sigma_t)_{avg}b(dc)cotan$ where $(\sigma_t)_{avg}=\frac{2M}{0.9bh^2}t$, $c = \frac{2M}{0.85f'cbh}t$

Note: concrete cylinder test $f'c$ was assumed as 0.8 times the concrete cube strength f_{cuf}.

II. METHODOLOGY

The methodology used in this study was carried out by ANSYS software based on the validation of the 7 equations presented in Table I [17-23]. A new approach will be adopted to simulate this vast amount of data. This approach will use the log file (Figure 5) to simulate and apply all the variables of the selected SFRC beams. These variables are: the ratio of shear span to the effective depth of the SFRC beam, compressive strength, longitudinal reinforcement ratio, volume fraction, aspect ratio, type of fiber.

III. EQUATIONS FOR THE SHEAR STRENGTH CAPACITY OF SFRC BEAMS

Several studies proposed equations that describe the shear capacity of SFRC beams. However, data analysis of previous studies indicates that the behavior of the SFRC beams remains a complicated issue. Therefore, all the suggested calculation methods for a shear load capacity of the beams are separated into the following three elements: (1) shear strength of the member without shear reinforcement which is found in the compression zone, longitudinal reinforcement, aggregate interlock (2) contribution of shear reinforcement, (3) contribution of steel fibers. Table I presents the most successful proposed equations that calculate the ultimate shear strength of SFRC beams without transverse reinforcement.

IV. MATERIAL MECHANICAL PROPERTIES

A. Concrete

In order to obtain an accurate finite element analysis, defining the modulus of elasticity, compressive behavior, and tension behavior of SFRC are essential. Therefore, this study extracted the stress-strain curves in tension and compression for the selected SFRC beams using the most famous available relationships for two types of fibers because the selected data involve straight and hooked-end steel fibers. Furthermore, an Excel sheet was prepared to predict the stress-strain curve for all simulated models.

1) The Behavior of the SFRC (Straight Fibers) in Compression

The contribution of steel fibers becomes more obvious after cracking. So the consequences of adding steel fibers appear clearly in the compressive behavior in the stress-strain curve of the SFRC beams. Volume fraction, geometry, and bond characteristics of steel fibers affect the compression behavior of the stress-strain curve. This contribution depends on the ability of concrete matrix with steel fibers to develop pull-out strength as the fibers provide crack-bridging function which allows to transverse the stress across the cracks and to arrest crack growth for already developed cracks [24-26]. However, the compressive strength is slightly increased when the matrix contains a low volume fraction of steel fibers. Authors in [27] proposed a formula to simulate the compressive stress-strain curve of concrete with straight steel fibers:

$$\sigma_c = f_{c.SF}\left[1 - \left(1 - \frac{\varepsilon_c}{\varepsilon_{co.CF}}\right)^2\right] \quad (1)$$

where $\varepsilon_{co.CF}$ is the strain value of the SFRC at the ultimate compressive stress. The first stage of the curve is assumed to

remain linear until 85% of $f_{c.SF}$. The other parameters corresponding to this point are calculated using the following expressions:

Strength value is:

$$f_{c.SF} = f_c(0.2315F + 1) \quad (2)$$

Strain at ultimate strength, $\varepsilon_{co.SF}$:

$$\varepsilon_{co.SF} = \varepsilon_{co}(0.95F + 1) \quad (3)$$

Ultimate strain:

$$\varepsilon_{cu.SF} = \varepsilon_{co.SF}(1.40F + 1) \quad (4)$$

where the *fc* is the cylinder compressive strength of concrete without steel fibers, ε_{co} is the maximum strain, usually assumed as 0.002. *F* is the fiber factor that depends on the geometry shape of the added steel fibers in the SFRC mixture, $F=\beta V_{SF}(l_{SF}/d_{SF})$, where β is the bond factor, equal to 0.5 for round shape, 0.75 for hooked, crimped, and undulated shapes, and 1.0 for indented shape, the V_{SF}, l_{SF}, and d_{SF} are the volume fraction, length, and diameter of the steel fibers, respectively.

2) The Behavior of the SFRC (Hooked End Fibers) in Compression

Using a high volume fraction of straight steel fibers results in workability difficulties. Therefore hooked end steel fibers have been used in many studies because this fiber geometry provides more pull-out resistance between the steel fibers and the matrix, which leads to obtaining better properties of SFRC by using fewer steel fibers to satisfy the workability requirements. The compressive behavior of the SFRC beams is significantly affected by the hooked end type. Adding hooked-end steel fibers to a concrete matrix enhances the deformation capability of the post-peak more than the straight type. Authors in [28] proposed an equation describing the compressive behavior of hooked-end SFRC.

$$\varepsilon_o = \left(0.0003V_f \frac{l_f}{d_f} + 0.0018\right) f_c'^{0.12} \quad (5)$$

$$E_c = \left(-367V_f \frac{l_f}{d_f} + 5520\right) f_c'^{0.41} \quad (6)$$

$$f_c = f_c' \left[\frac{A(\varepsilon_c/\varepsilon_o)}{A-1+(\varepsilon_c/\varepsilon_o)^B}\right] \quad (7)$$

$$A = B = \frac{1}{1-\left(\frac{f_c'}{\varepsilon_o E_c}\right)} \; for \; \varepsilon_c/\varepsilon_o \leq 1.0 \quad (8)$$

$$A = 1 + 0.723\left(V_f \frac{l_f}{d_f}\right)^{-0.882} \text{ for } \varepsilon_c/\varepsilon_o > 1.0 \quad (9)$$

$$B = \left(\frac{f_c'}{50}\right)^{0.064}\left[1 + 0.882\left(V_f \frac{l_f}{d_f}\right)^{-0.882}\right] > A$$

in (6) for $\varepsilon_c/\varepsilon_o > 1.0$ (10)

B. Tensile Behavior of the SFRC

Many analytical stress-strain expressions have been derived from previous studies to identify and determine the SFRC behavior during tension. In this research, a smeared crack method that has previously been adopted in many studies has been used in this study to extract the behavior of SFRC concrete under tension for the selected data. The total tensile strain, ε_t, is the sum of an elastic, $\varepsilon_{t,el}$, and a fracture component, $\varepsilon_{t,fr}$, that can be estimated based on the following:

$$\varepsilon_t = \varepsilon_{t,el} + \varepsilon_{t,fr} \quad (11)$$

$$\varepsilon_{t,el} = \sigma_t / E_{t,SF} \quad (12)$$

$$\varepsilon t_{,fr} = wt / L_{fr,SF} \quad (13)$$

where σ_t is the tensile stress of SFRC, $E_{t,SF.}$ is the modulus of elasticity under the tension of SFRC, w_t is the crack width, and $L_{fr,SF}$ is the length of the SFRC.

Although the previous equations will produce the stress-strain curve for both hardening and softening regions for SFRC under compression and tension stresses, it is important to explain that the ANSYS software deals only with the hardening region in the stress-strain curve, either in compression or tension (red and blue colored region in Figure 1) and the softening part after the colored region will not be considered, according to the fact that the ANSYS does not need more than one point to identify the tensile stress-strain curve (Table II). The hardening region in the tensile stress-strain curve of concrete shows linear behavior under the tension stress for a low dosage of steel fibers is used because the addition of high dosage leads to high residual stress of bending or direct tensile stress tests. Also, the effect of added steel fibers to concrete appears after the cracking of the concrete matrix [29]. In contrast, regarding the compression stress-strain of concrete, there are two regions to identify the compression behavior of concrete.

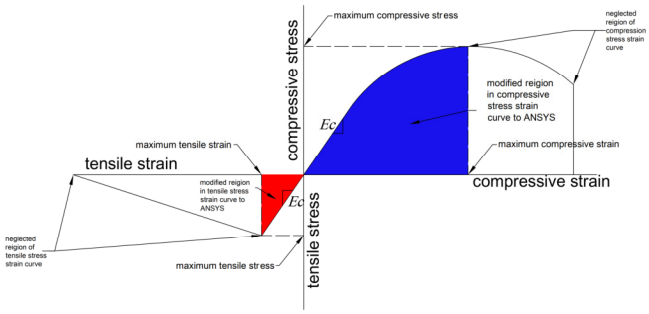

Fig. 1. The modified region of concrete stress-strain curve in ANSYS.

The region beyond the elastic limit in the compressive stress-strain curve represents the first point to be entered in ANSYS, and the last point is the maximum compressive stress. Therefore an Excel sheet was prepared to identify and select the intended part from the compressive stress-strain curve to model the SFRC beams, see Figure 2.

C. Steel Rebars

Steel rebars are assumed to be bilinear isotropic in this study. Their elastic modulus of elasticity is 200000 MPa and Poisson's ratio is 0.3. The bilinear model requires the yield stress (*fy*), and in some beams, the hardening modulus of steel rebars has to be defined [30, 31].

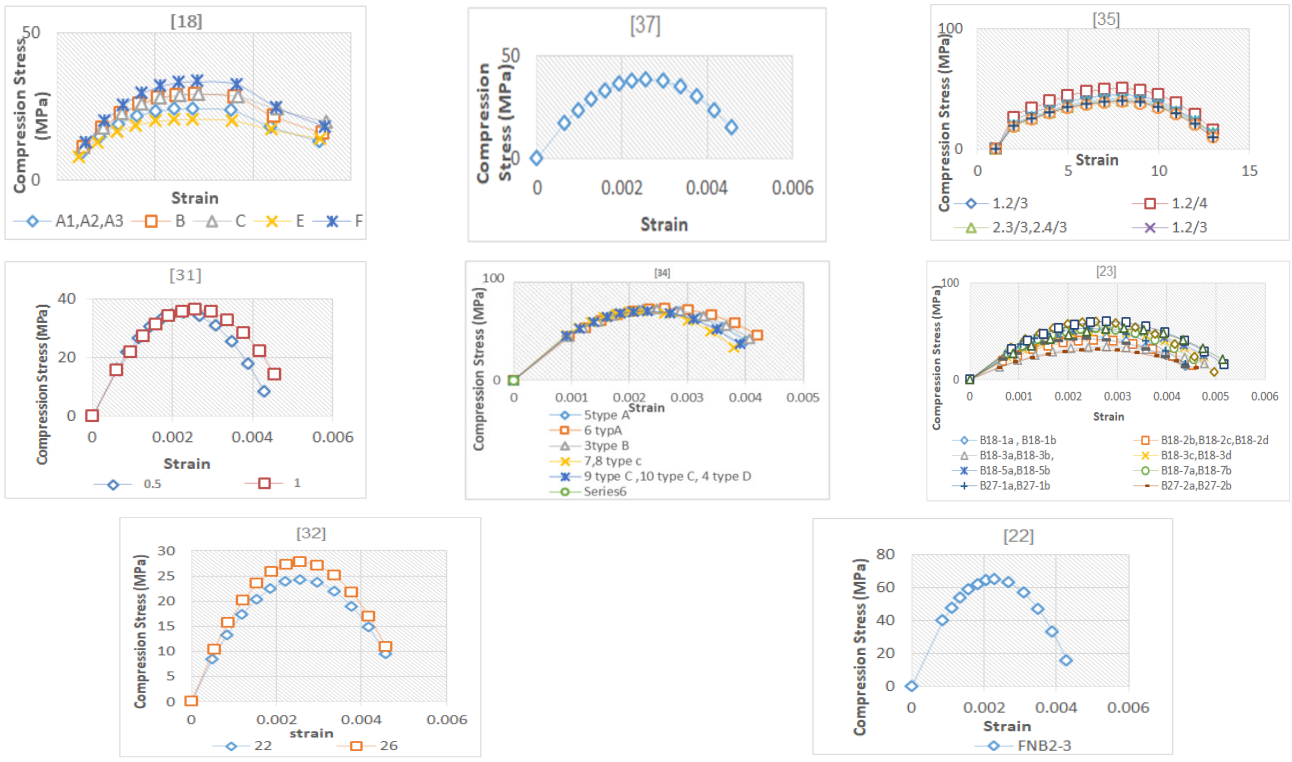

Fig. 2. The compressive stress-strain curves of SFRC beams.

D. Steel Bearing Plate

Steel plates are usually placed at support locations of the tested beams and under two point loads in the finite element models to provide the stress distribution over the support areas and prevent a local failure of the model. The modulus of elasticity for the steel is 200000 MPa and Poisson's ratio is 0.3.

V. MATERIAL MODELING IN ANSYS

A. Concrete

The solid element SOLID65 is used to model the concrete in ANSYS. This element has 8 nodes with 3 degrees of freedom for each node in *x*, *y*, and *z* directions. The element is capable of plastic deformation and cracking in 3 orthogonal directions.

B. Steel Rebar

For the steel reinforcement rebars, the beam element 188 was used between two nodes. This element provides an easier and more accurate change of area steel.

C. Steel Plates

Steel plates were modeled by using element Soild185. This element is defined by 8 nodes with three 3 of freedom.

D. Simulation by Log File Feature of ANSYS

Authors in [11] used the classical approach. In this study, using the log file of ANSYS provides many benefits in the studies with many parameters and variables, since one log file can simulate and modify all physical and mechanical properties. For example, the selected 91 SFRC beams of the current study were simulated by one log file involving all their parameters and variables that could be processed by a text editor and new command lines could be added to describe the input information. However, using finite element software with vast data in high definition has many challenges. Therefore, in terms of compaction, the log file was considered as the best approach to simulate the beams in this study. Also, this file involves all records of the commands and steps used during the simulation. Furthermore, since the log file is written in text format, it is easy to transfer from one machine to another and use it to solve errors and do further analysis. Table II contains all the required information, such as the physical and material properties of the selected data. These data have been modeled to correspond to one log file, as this log file involves all physical properties of bearing steel plates, steel rebars, and boundary conditions of the SFRC beam. As shown in Figure 3, changing model geometry is effortless when we depend on these features. For example, the geometry of selected data, such as beam dimensions and rebar's radius of any selected beam are reachable without creating a new job as in conventional simulation approaches. The Figure also explains the lines in the log file responsible for modifying the other physical properties, such as the modulus of elasticity, Poisson's ratio, etc. For control mesh size in a regular geometry, the manual meshing of a block has been used. However, cutting the line of entities of the solid in 3 dimensions is more practical than applying distance, so it computes element edges in 3 dimensions by these cut lines. This method is used because the dimensions of the beams in the selected data are different and error messages will appear.

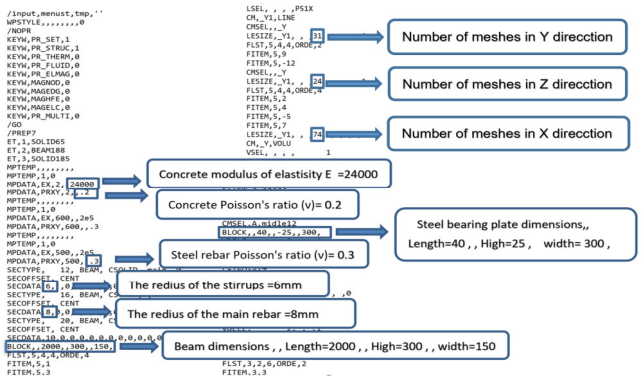

Fig. 3. The log file.

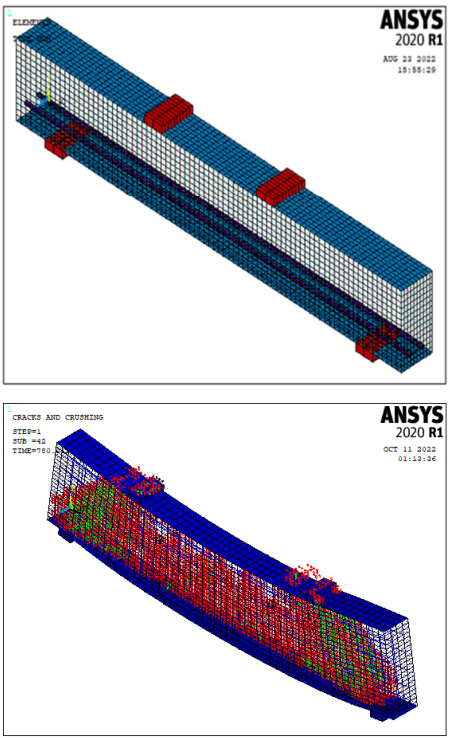

Fig. 4. (a) Assembly of concrete, steel rebar and bearing plates, (b) crack pattern.

Figure 4 shows the finite element representation for SFRC concrete and steel reinforcement simulation of the selected beams. All elements had a mesh of the same size therefore every used material shares the same node. The boundary conditions are represented as hinge and roller support. These supports have been simulated by an individual line of nodes created on a steel plate located under the applied load points and support zones. In hinge support, the selected nodes were constrained for UX, UY, and UZ displacement, while in the roller support, the selected nodes were constrained in UY and UZ displacement. The steel plates were used for a better distribution of the stresses in the applied load points and support areas. The intelligent method of meshing was used to mesh the entire model entities. Hexahedral elements were used.

VI. COMPARISON AMONG THE PROPOSED SHEAR EQUATIONS

A total 91 concrete SFRC beams were analyzed in ANSYS program. Many researchers have proposed analytical equations to calculate the ultimate shear capacity of SFRC beams based on the results of experimental investigations. The performance and accuracy of the extracted results of ANSYS need to be evaluated with the results of experimental tests and the proposed equations of Table I. Most proposed equations comprise the term fibre factor *F*, which collects the effect of the fiber aspect ratio *A* and volume fraction V_f on the shear strength of SFRC beams. The accuracy of the extracted results from the used equations was compared based on descriptive statistical analysis. Two statistical parameters were used in the comparison: (a) χ factor, which is the inverse of the slope of a linear least-square regression of the experimental work (*Vexp*) versus the calculated shear strength (*Vcal*) predicted either by formula or finite element analysis and (b) Absolute Error (AE), which is calculated by (7):

$$\text{AE} = \frac{V_{u.\ exp} - V_{u.\ pre}}{V_{u.\ exp}} \quad (7)$$

where $V_{u.\ exp}$ is the experimental ultimate shear capacity (kN), and $V_{u.\ pre}$ is the predicted shear strength (kN).

According to the analysis results of Figure 5, the χ value of [23] was the closest result to the experimental value among the seven equations, while [17] gave the furthest. Conversely, the χ value of [22] and ANSYS is 0.91 and 98, respectively. The predicted shear strength capacity values for the SFRC beams along with the ANSYS results of this study are listed in Table II. The results of ANSYS are more close to the experimental results because the finite element theory can estimate the load failure capacity for any failure. A good agreement was found between the derived shear equations and ANSYS software results of shear strengths for the tested beams. The AE factors of the closest of the considered equations and ANSYS software shear are 45and 34, respectively.

VII. CONCLUSIONS

The main conclusions derived from the obtained results of the current study are:

- Adding steel fibers to normal concrete causes dramatic changes in the behavior of the stress-strain curve, therefore, shear capacity will withstand a considerable change. However, this change depends on the aspect ratio and volume fraction of the steel fibers.
- The equation from [22] that predicts shear capacity gives the closest results to the experimental χ while the equation from [17] predicted the furthest value.
- The contribution of steel fibers on the shear strength capacity of SFRC beams by fibres bridging diagonal cracks can be reasonably estimated for beams along the compression and tension zone while neglecting the contribution of aggregate interlock and steel reinforcement.

TABLE II. COMPARISON OF THE EXPERIMENTAL AND THE DERIVED SHEAR CAPACITY EQUATIONS WITH ANSYS

Beam	*bw* mm	*h* mm	*d* mm	*a/d*	*ρ* %	*Vf* %	*f 'c'* MPa	$V_{u,exp}$ (kN)	$V_{u,pre}$ (kN)	$\frac{\lvert V_{u.exp} - V_{u.\,pre}\rvert}{V_{u.exp}}$	$V_{u.\,ANSYS}$ (kN)	$\frac{\lvert V_{u.exp} - V_{u.}}{V_{exp}}$
A2	152	229	197	2.8	1.3	—	24.2	44.192	18.12[6]	14	46.3	5
A3	152	229	197	3.6	1.3	—	24.2	38.299	20.30[6]	24	41.2	8
A4	152	229	197	4.4	1.3	—	24.2	33.88	22.36[6]	19	36	6
B2	152	229	197	2.8	1.3	0.50	29.1	51.69	44.97[3]	6	61.54	19
B3	152	229	197	3.6	1.3	0.50	29.1	45.229	47.49[1]	3	52.17	15
C2	152	229	197	2.8	1.3	0.750	29.9	60.582	53.31[3]	3	66.1	9
C6	152	229	197	2.8	2.0	0.750	29.9	65.495	54.36[3]	2	69.9	7
E2	152	229	197	2.8	1.3	0.750	20.6	44.849	45.75[1]	0	42.6	5
E3	152	229	197	2.8	2.0	0.750	20.6	59.799	49.63[3]	1	63.53	6
F3	152	229	197	2.8	2.0	0.750	33.4	86.527	61.43[6]	8	91.1	5
2/0.5/2.5	152	254	221	2.5	1.2	0.51	34.0	58.762	50.54[3]	8	53.18	9
2/0/3.5	152	254	221	3.5	1.2	—	34.0	39.175	18.80[6]	5	42.17	8
4/0.5/2.5	152	254	221	2.5	2.4	0.51	34.0	62.679	50.77[4]	0	66.11	5
4/0.5/3.5	152	254	221	3.5	2.4	0.51	34.0	48.968	51.91[5]	4	51.33	5
4/0/3.5	152	254	221	3.5	2.4	—	34.0	35.257	16.92[1]	5	35.43	0
4/1.0/2.5	152	254	221	2.5	2.4	0.51	34.0	82.267	67.46[2]	0	81.51	1
4/1.0/3.5	152	254	221	3.5	2.4	0.51	34.0	66.597	68.59[7]	3	43.96	34
—	127	229	203	3.0	2.2	—	17.8	42.42	19.94[2]	4	36.44	14
—	127	229	203	3.0	2.2	0.50	22.7	78.613	56.60[6]	18	85.53	9
—	127	229	203	3.0	2.2	0.50	26.0	78.875	58.37[3]	2	74.07	6
HSFRC1	127	254	225	2.9	3.6	0.50	68.9	156.55	100.19[6]	20	74.86	7
HSFRC2	127	254	225	2.9	3.6	0.50	68.9	156.55	100.19[6]	19	77.66	21
HSFRC3	127	254	225	2.9	2.2	0.50	68.9	99.62	80.69[3]	3	77.19	23
1 type A	200	250	180	3.3	4.5	—	68.9	212.16	106.08[2]	45	200.9	5
5 type A	200	250	180	3.3	4.5	0.70	68.9	251.01	148.10[7]	41	266	6
6 type A	200	250	180	3.3	4.5	0.70	68.9	262.96	160.41[7]	39	272.3	4
1 type B	200	300	235	2.8	4.3	—	68.9	280.89	112.36[2]	43	288	3
3 type B	200	300	235	2.8	4.3	0.60	68.9	308.2	172.59[6]	35	311.4	1
1 type C	200	500	410	2.9	3.0	—	68.9	176.97	70.79[3]	6	191.54	8
7 type C	200	500	410	2.9	3.0	0.70	68.9	265.45	177.85[2]	4	255.1	11
8 type C	200	500	410	2.9	3.0	0.70	68.9	313.1	194.12[6]	4	310.7	1
9 type C	200	500	410	2.9	3.0	0.70	68.4	339.09	213.63[6]	3	349.6	6
10 type C	200	500	410	2.9	3.0	0.70	68.9	292.68	201.95[3]	5	300.1	11
4 type D	300	700	570	3.0	2.9	0.70	68.4	509.13	381.85[1]	5	525.9	9
FHB1-3	127	254	213	3.0	1.5	—	62.6	68.489	28.77[6]	22	81.8	19
FHB1-4	127	254	213	4.0	1.5	—	62.6	53.507	29.96[6]	20	62.6	17
FNB2-3	127	254	213	3.0	1.5	0.80	30.8	69.058	49.72[2]	13	77.1	12
1.2/1	200	300	260	3.5	3.6	—	44.0	89.682	43.94[3]	5	96.4	7
1.2/3	200	300	260	3.5	3.6	0.90	43.7	120.31	99.86[3]	3	133	11
1.2/4	200	300	260	3.5	3.6	0.90	48.3	155.4	122.76[6]	3	163.78	5
2.3/1	200	300	262	2.5	1.2	—	40.1	79.637	27.08[3]	14	70.3	12
2.3/3	200	300	262	2.5	1.2	0.90	38.7	107.57	91.44[1]	0	111.31	22
2.4/1	200	300	260	2.5	1.8	—	40.1	118.54	42.68[6]	8	119.3	1
2.4/3	200	300	260	2.5	1.8	0.90	38.7	142.33	99.63[2]	6	155.6	9
2.6/1	200	300	260	4.0	1.8	—	40.8	76.394	43.54[6]	7	77	3
2.6/3	200	300	260	4.0	1.8	0.90	40.3	115.54	112.07[6]	1	113.9	1
20 × 30-Plain-1	200	300	260	3.5	2.8	—	32.1	58.923	28.87[1]	1	61.3	4
20 × 30-SFRC-1	200	300	260	3.5	2.8	0.90	37.7	111.75	96.10[3]	1	109.1	17
20 × 45-SFRC-1	200	450	410	3.3	3.1	0.90	37.7	146.01	137.25[1]	3	144.6	1
20 × 60-Plain-1	200	600	540	3.5	2.7	—	32.1	110.14	53.97[5]	5	123.5	12
T 10 × 50-SFRC-1	200	500	460	3.4	2.8	0.90	37.7	169.46	155.91[1]	2	179.5	6
T 15 × 50-SFRC-1	200	500	460	3.4	2.8	0.90	37.7	265.5	196.47[2]	1	274	7
T 15 × 75-SFRC-1	200	500	460	3.4	2.8	0.90	37.7	259.85	194.88[2]	15	265.9	14
T 15 × 100-Plain-1	200	500	460	3.4	2.8	—	32.1	151.16	74.07[6]	11	144.3	5
*T*15 × 100-SFRC-1	200	500	460	3.4	2.8	0.90	37.7	242.9	184.60[2]	10	234.6	3
20 × 30-SFRC-2	200	300	260	3.5	2.8	0.90	38.8	132.8	106.24[2]	5	131	16
20 × 50-SFRC-2	200	500	460	3.4	2.4	0.90	38.8	149	149.00[7]	0	157.7	6
20 × 60-SFRC-2	200	600	540	3.5	2.7	0.90	38.8	222	195.36[3]	2	234	5
T 10 × 50-SFRC-2	200	500	460	3.4	2.8	0.90	38.8	154.73	148.54[7]	4	147.5	5
T 15 × 50-SFRC-2	200	500	460	3.4	2.8	0.90	38.8	160.46	150.83[1]	3	161.1	0
T 23 × 50-SFRC-2	200	500	460	3.4	2.8	0.90	38.8	252.15	189.11[2]	12	277	10
A00	150	249	218	2.8	1.9	—	41.2	39.88	15.15[1]	2	33.8	15
A10	150	249	218	2.8	1.9	0.51	40.9	96.198	73.11[6]	3	104.9	9
A20	150	249	218	2.8	1.9	0.51	43.2	103.16	89.75[5]	2	111.77	8
B18-0a	152	457	381	3.4	2.7	—	42.8	64.408	30.27[5]	2	64.9	1
B18-0b	152	457	381	3.4	2.7	—	42.8	64.408	30.27[5]	1	66.3	3
B18-1a	152	457	381	3.4	2.0	0.55	44.8	170.55	131.33[2]	12	183.32	7
B18-1b	152	457	381	3.4	2.0	0.55	44.8	158.92	125.55[2]	6	167.3	5
B18-2a	152	457	381	3.5	2.0	0.55	38.1	175.16	136.62[2,6,7]	22	171.6	2
B18-2b	152	457	381	3.5	2.0	0.55	38.1	178.73	137.62[2,6,7]	23	176.8	1
B18-2c	152	457	381	3.5	2.7	0.55	38.1	200.18	148.13[6,7]	26	221.1	10
B18-2d	152	457	381	3.5	2.7	0.55	38.1	146.56	124.58[6]	1	16.8	10

Beam	*bw* mm	*h* mm	*d* mm	*a/d*	*ρ* %	*Vf* %	*f 'c'* MPa	$V_{u,exp}$ (kN)	$V_{u,pre}$ (kN)	$\frac{\lvert V_{u.exp} - V_{u.\,pre}\rvert}{V_{u.exp}}$	$V_{u.\,ANSYS}$ (kN)	$\frac{\lvert V_{u.exp} - V_{u.}\rvert}{V_{exp}}$
B18-3a	152	457	381	3.4	2.7	0.55	31.0	148.32	126.07[4]	4	149.1	1
B18-3b	152	457	381	3.4	2.7	0.55	31.0	196.69	149.48[3]	14	207.2	7
B18-3c	152	457	381	3.4	2.7	0.55	44.9	190.15	146.41[3,6]	5	201.8	6
B18-3d	152	457	381	3.4	2.7	0.55	44.9	190.15	146.41[6]	4	201.6	6
B18-5a	152	457	381	3.4	2.7	0.75	49.2	170.61	133.07[1]	1	177.4	10
B18-5b	152	457	381	3.4	2.7	0.75	49.2	219.35	155.74[6]	16	213.6	3
B18-7a	152	457	381	3.4	2.0	0.38	43.3	190.54	139.09[2]	23	178.5	6
B18-7b	152	457	381	3.4	2.0	0.38	43.3	186.73	138.18[6]	21	174.8	6
B27-1a	203	686	610	3.5	2.1	0.55	50.8	361.86	278.63	6	347.5	4
B27-1b	203	686	610	3.5	2.1	0.55	50.8	335.38	268.31[2]	2	350	7
B27-2a	203	686	610	3.5	2.1	0.75	28.7	344.96	269.07[3,6]	18	533.8	8
B27-2b	203	686	610	3.5	2.1	0.75	28.7	338.33	267.28[6]	16	330.3	2
B27-3a	203	686	610	3.5	1.6	0.55	42.3	338.26	270.60[2]	8	330	2
B27-3b	203	686	610	3.5	1.6	0.55	42.3	346.31	273.58	10	334.76	3
B27-4a	203	686	610	3.5	1.6	0.75	29.6	262.75	231.22[2,3,6]	2	275.5	5
B27-4b	203	686	610	3.5	1.6	0.75	29.6	222.32	217.88[3]	1	231.2	4
B27-5	203	686	610	3.5	2.1	0.55	44.4	429.06	326.09[3,6]	16	457.3	7
B27-6	203	686	610	3.5	2.1	0.75	42.8	421.26	324.37[1]	2	440.4	5
B27-7	203	686	610	3.5	1.6	—	37.0	158.18	77.51[6]	2	169.3	7

[1] [19]; [2] [18]; [3] [20]; [4] [21]; [5] [22]; [6] [23]; and [7] [24]

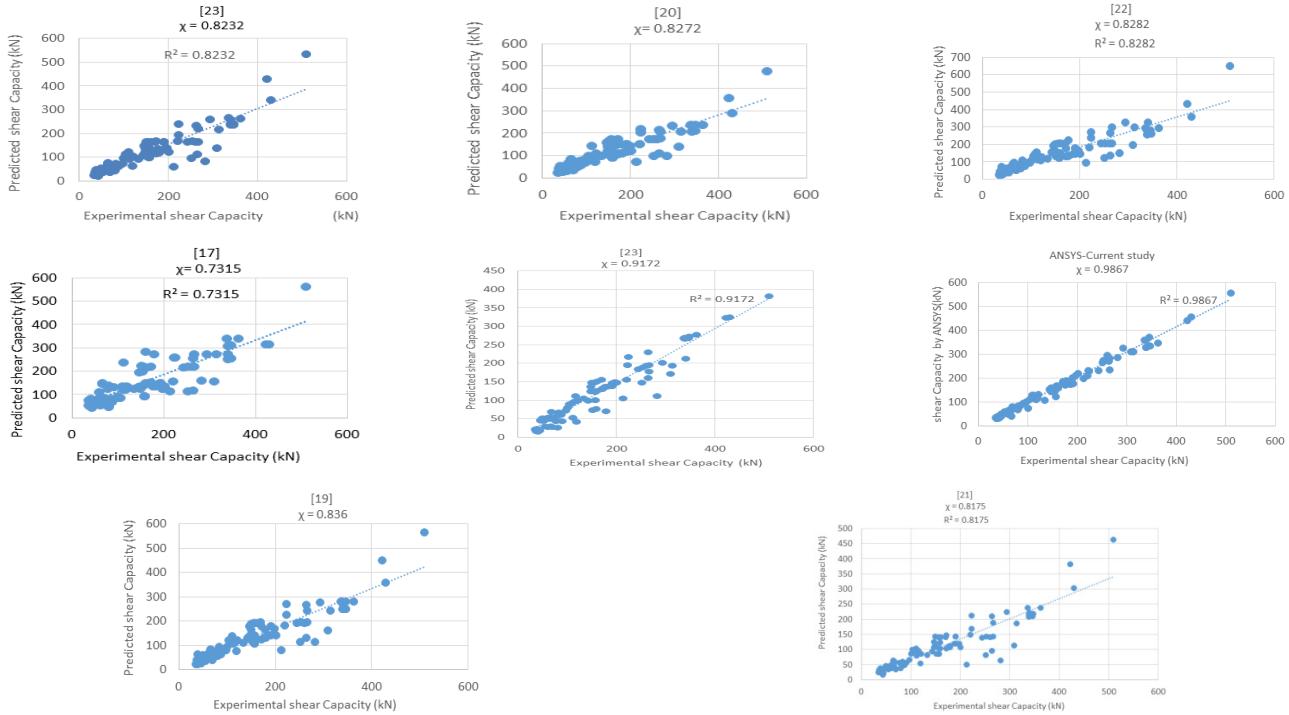

Fig. 5. χ factor value (R-squared value of experimental shear to predicted shear) of the selected data.

- The results obtained from ANSYS were more correlated to the more reliable experimental results. Therefore the modeling made with ANSYS can reduce cost and save time. Also, the errors that can be made in the design stage or wrong material selection can be prevented, therefore, this method can guide further experimental studies.
- This approach of simulations in ANSYS allows the simulation of many SFRC beams, therefore the predicted equations of shear capacity will be more accurate than the derived experimental or analytical equations.
- This approach provides the ability to derive the most accurate equation to predict the shear capacity of the SFRC beams, as it is easy to modify the physical properties of SFRC in the text lines of the log file, to simulate a large number of SFRC beams not involved in the experimental work.
- Finally, this method will allow studying the effect of more variables that had not been discussed in precious studies and derive more accurate equations to determine either shear or flexural capacity.

REFERENCES

[1] ACI Committee 544, *ACI PRC-544.5-10: Report on the Physical Properties and Durability of Fiber-Reinforced Concrete*. American Concrete Institute, 2010.

[2] ACI Committee 544, *ACI PRC-544.4-18: Guide to Design with Fiber-Reinforced Concrete*. American Concrete Institute, 2018.

[3] ACI Committee 544, *544.1R-96 - Report On Fiber-Reinforced Concrete*. American Concrete Institute, 2001.

[4] W. A. Labib, "Evaluation of hybrid fibre-reinforced concrete slabs in terms of punching shear," *Construction and Building Materials*, vol. 260, Nov. 2020, Art. no. 119763, https://doi.org/10.1016/j.conbuildmat.2020.119763.

[5] V. Sathish Kumar, N. Ganesan, and P. V. Indira, "Shear Strength of Hybrid Fibre-Reinforced Ternary Blend Geopolymer Concrete Beams under Flexure," *Materials*, vol. 14, no. 21, Jan. 2021, Art. no. 6634, https://doi.org/10.3390/ma14216634.

[6] J. V. Jenifer, D. Brindha, J. V. Jenifer, and D. Brindha, "Development of hybrid steel-basalt fiber reinforced concrete - in aspects of flexure, fracture and microstructure," *Revista de la construcción*, vol. 20, no. 1, pp. 62–90, Apr. 2021, https://doi.org/10.7764/rdlc.20.1.62.

[7] Adanagouda, H. M. Somasekharaiah, M. S. Shobha, and H. M. Mallikarjuna, "Combined effect of metakaolin and hybrid fibers on the strength properties of high performance concrete," *Materials Today: Proceedings*, vol. 49, pp. 1527–1536, Jan. 2022, https://doi.org/10.1016/j.matpr.2021.07.310.

[8] M. A. J. Hassan and A. F. Izzet, "Experimental and Numerical Comparison of Reinforced Concrete Gable Roof Beams with Openings of Different Configurations," *Engineering, Technology & Applied Science Research*, vol. 9, no. 6, pp. 5066–5073, Dec. 2019, https://doi.org/10.48084/etasr.3188.

[9] F. J. Alkhafaji and A. F. Izzet, "Prestress Losses in Concrete Rafters with Openings," *Engineering, Technology & Applied Science Research*, vol. 10, no. 2, pp. 5512–5519, Apr. 2020, https://doi.org/10.48084/etasr.3390.

[10] A. M. Al-Hilali, A. F. Izzet, and N. Oukaili, "Static Shear Strength of a Non-Prismatic Beam with Transverse Openings," *Engineering, Technology & Applied Science Research*, vol. 12, no. 2, pp. 8349–8353, Apr. 2022, https://doi.org/10.48084/etasr.4789.

[11] D. H. Lee, J.-H. Hwang, H. Ju, K. S. Kim, and D. A. Kuchma, "Nonlinear finite element analysis of steel fiber-reinforced concrete members using direct tension force transfer model," *Finite Elements in Analysis and Design*, vol. 50, pp. 266–286, Mar. 2012, https://doi.org/10.1016/j.finel.2011.10.004.

[12] H.-B. Ly, T.-T. Le, H.-L. T. Vu, V. Q. Tran, L. M. Le, and B. T. Pham, "Computational Hybrid Machine Learning Based Prediction of Shear Capacity for Steel Fiber Reinforced Concrete Beams," *Sustainability*, vol. 12, no. 7, Jan. 2020, Art. no. 2709, https://doi.org/10.3390/su12072709.

[13] A. Marì Bernat, N. Spinella, A. Recupero, and A. Cladera, "Mechanical model for the shear strength of steel fiber reinforced concrete (SFRC) beams without stirrups," *Materials and Structures*, vol. 53, no. 2, Feb. 2020, Art. no. 28, https://doi.org/10.1617/s11527-020-01461-4.

[14] L. N. Hussain, A. S. Mohammed, and A. A. Mansor, "Finite Element Analysis of Large-Scale Reinforced Concrete Shell of Domes," *Journal of Engineering Science and Technology*, vol. 15, no. 4, pp. 2712–2729, 2020.

[15] *ANSYS Modeling and Meshing Guide*. Canonsburg, PA, USA: ANSYS, 2010.

[16] A. Sader Mohammed and L. Hussain, "Finite Element Modeling for Self-Compacting Reinforced Concrete Deep Beams Containing Web Openings," *International Journal of Engineering & Technology*, vol. 7, no. 4.20, pp. 546–552, Nov. 2018, https://doi.org/10.14419/ijet.v7i4.20.26416.

[17] A. K. Sharma, "Shear Strength of Steel Fiber Reinforced Concrete Beams," *Journal Proceedings*, vol. 83, no. 4, pp. 624–628, Jul. 1986, https://doi.org/10.14359/10559.

[18] M. A. Mansur, K. C. G. Ong, and P. Paramasivam, "Shear Strength of Fibrous Concrete Beams Without Stirrups," *Journal of Structural Engineering*, vol. 112, no. 9, pp. 2066–2079, Sep. 1986, https://doi.org/10.1061/(ASCE)0733-9445(1986)112:9(2066).

[19] R. Narayanan and I. Y. S. Darwish, "Use of Steel Fibers as Shear Reinforcement," *ACI Structural Journal*, vol. 84, no. 3, pp. 216–227, May 1987, https://doi.org/10.14359/2654.

[20] S. A. Ashour, G. S. Hasanain, and F. F. Wafa, "Shear Behavior of High-Strength Fiber Reinforced Concrete Beams," *ACI Structural Journal*, vol. 89, no. 2, pp. 176–184, Mar. 1992, https://doi.org/10.14359/2946.

[21] M. Khuntia, B. Stojadinovic, and S. C. Goel, "Shear Strength of Normal and High-Strength Fiber Reinforced Concrete Beams without Stirrups," *ACI Structural Journal*, vol. 96, no. 2, pp. 282–289, Mar. 1999, https://doi.org/10.14359/620.

[22] Y.-K. Kwak, M. O. Eberhard, W.-S. Kim, and J. Kim, "Shear Strength of Steel Fiber-Reinforced Concrete Beams without Stirrups," *ACI Structural Journal*, vol. 99, no. 4, pp. 530–538, Jul. 2002, https://doi.org/10.14359/12122.

[23] H. H. Dinh, G. J. Parra-Montesinos, and J. K. Wight, "Shear Strength Model for Steel Fiber Reinforced Concrete Beams without Stirrup Reinforcement," *Journal of Structural Engineering*, vol. 137, no. 10, pp. 1039–1051, Oct. 2011, https://doi.org/10.1061/(ASCE)ST.1943-541X.0000362.

[24] T. Li *et al.*, "Structural behaviors of steel fiber-reinforced concrete-filled geotextile tube stub columns under axial compression," *Structures*, vol. 40, pp. 434–447, Jun. 2022, https://doi.org/10.1016/j.istruc.2022.04.047.

[25] N. Majain, A. B. Abd. Rahman, A. Adnan, and R. N. Mohamed, "Bond behaviour of deformed steel bars in steel fibre high-strength self-compacting concrete," *Construction and Building Materials*, vol. 318, Feb. 2022, Art. no. 125906, https://doi.org/10.1016/j.conbuildmat.2021.125906.

[26] J. Carrillo, J. A. Pincheira, and J. Abellán-García, "Direct Tension Tests of Concrete Reinforced with Hooked Steel Fibers," *Materials Journal*, vol. 119, no. 6, pp. 77–89, Nov. 2022, https://doi.org/10.14359/51737186.

[27] C. E. Chalioris, "Analytical approach for the evaluation of minimum fibre factor required for steel fibrous concrete beams under combined shear and flexure," *Construction and Building Materials*, vol. 43, pp. 317–336, Jun. 2013, https://doi.org/10.1016/j.conbuildmat.2013.02.039.

[28] S.-C. Lee, J.-H. Oh, and J.-Y. Cho, "Compressive Behavior of Fiber-Reinforced Concrete with End-Hooked Steel Fibers," *Materials*, vol. 8, no. 4, pp. 1442–1458, Apr. 2015, https://doi.org/10.3390/ma8041442.

[29] W.-F. Chen, *Plasticity in Reinforced Concrete*. Ft. Lauderdale, FL, USA: J. Ross Publishing, 2007.

[30] I. Sæther and B. Sand, "FEM simulations of reinforced concrete beams attacked by corrosion," *NCR*, vol. 39, no. 2, pp. 15–31, Jun. 2012.

[31] T. Y. Lim, P. Paramasivam, and S. L. Lee, "Shear and moment capacity of reinforced steel-fibre-concrete beams," *Magazine of Concrete Research*, vol. 39, no. 140, pp. 148–160, Sep. 1987, https://doi.org/10.1680/macr.1987.39.140.148.

[32] V. C. Li, R. Ward, and A. M. Hmaza, "Steel and Synthetic Fibers as Shear Reinforcement," *Materials Journal*, vol. 89, no. 5, pp. 499–508, Sep. 1992, https://doi.org/10.14359/1822.

[33] P. Casanova and P. Rossi, "High-Strength Concrete Beams Submitted to Shear: Steel Fibers Versus Stirrups," *ACI Special Publication*, vol. 182, pp. 53–68, May 1999, https://doi.org/10.14359/5521.

[34] K. Noghabai, "Beams of Fibrous Concrete in Shear and Bending: Experiment and Model," *Journal of Structural Engineering*, vol. 126, no. 2, pp. 243–251, Feb. 2000, https://doi.org/10.1061/(ASCE)0733-9445(2000)126:2(243).

[35] J. Rosenbusch and M. Teutsch, "Trial beams in shear Brite/Euram Project 97-4163," Technical University of Braunschweig, Braunschweig, Germany, Final Report, 2003.

[36] C. Cucchiara, L. La Mendola, and M. Papia, "Effectiveness of stirrups and steel fibres as shear reinforcement," *Cement and Concrete Composites*, vol. 26, no. 7, pp. 777–786, Oct. 2004, https://doi.org/10.1016/j.cemconcomp.2003.07.001.

[37] K. H. Tan, K. Murugappan, and P. Paramasivam, "Shear Behavior of Steel Fiber Reinforced Concrete Beams," *ACI Structural Journal*, vol. 90, no. 1, pp. 3–11, Feb. 1993.